nature protocols

https://doi.org/10.1038/s41596-023-00848-1

Protocol

Check for updates

# Microlensed fiber allows subcellular imaging by laser-based mass spectrometry

Yifan Meng [1,2], Wei Hang [1] ✉ & Richard N. Zare [2] ✉

## Abstract

Mass spectrometry imaging (MSI) enables the chemical mapping of molecules and elements in a label-free, high-throughput manner. Because this approach can be accomplished rapidly, it also enables chemical changes to be monitored. Here, we describe a protocol for MSI with subcellular spatial resolution. This is achieved by using a microlensed fiber, which is made by grinding an optical fiber. It is a universal and economic technique that can be adapted to most laser-based mass spectrometry methods. In this protocol, the output of laser radiation from the microlensed fiber causes laser ablation of the sample, and the resulting plume is mass spectrometrically analyzed. The microlensed fiber can be used with matrix-assisted laser desorption ionization, laser desorption ionization, laser ablation electrospray desorption ionization and laser ablation inductively coupled plasma, in each case to achieve submicroscale imaging of single cells and biological tissues. This report provides a detailed introduction of the microlensed fiber design and working principles, sample preparation, microlensed fiber ion source setup and multiple MSI platforms with different kinds of mass spectrometers. A researcher with a little background (such as a trained graduate student) is able to complete all the steps for the experimental setup in ~2 h, including fiber test, laser coupling and ion source modification. The imaging time spent mainly depends on the size of the imaging area. It is suggested that most existing laser-based MSI platforms, especially atmospheric pressure applications, can achieve breakthroughs in spatial resolution by introducing a microlensed fiber module.

## Key points

- A microlens capable of focusing laser radiation is formed by rounding one end of an optical fiber. Focusing light on smaller spots improves the resolution of laser desorption or ablation sample surfaces, making nanoscale mass spectrometry imaging analysis possible.
- Microlensed fibers can be incorporated into matrix-assisted laser desorption ionization, laser desorption ionization, laser ablation electrospray desorption ionization and laser ablation inductively coupled plasma setups.

## Key references

Meng, Y. et al. *Angew. Chem. Int. Ed. Engl.* **59**, 17864–17871 (2020): https://doi.org/10.1002/anie.202002151

Meng, Y. et al. *ACS Nano* **15**, 13220–13229 (2021): https://doi.org/10.1021/acsnano.1c02922

Meng, Y. et al. *Anal. Chem.* **94**, 10278–10282 (2022): https://doi.org/10.1021/acs.analchem.2c01942

[1]Ministry of Education (MOE) Key Laboratory of Spectrochemical Analysis and Instrumentation, College of Chemistry and Chemical Engineering, Xiamen University, Xiamen, China. [2]Department of Chemistry, Stanford University, Stanford, CA, USA. ✉e-mail: weihang@xmu.edu.cn; zare@stanford.edu

## Introduction

The visualization of chemical distributions in microscale biological samples, such as tissues and cells, is important for chemistry and bioscience research. Mass spectrometry (MS) imaging (MSI) has become a popular analytical method for biological mapping, because highly sensitive, label-free analysis is possible[1–10]. Laser ablation and desorption are two of the most common in situ sampling methods that are used in combination with different MS techniques. MSI techniques that rely on the use of lasers include laser desorption ionization (LDI)-MS[11–13], matrix-assisted laser desorption ionization (MALDI)-MS[14–16], laser ablation inductively coupled plasma (ICP) (LA-ICP)-MS[17–19] and laser ablation electrospray ionization (LA-ESI)-MS[20–22]. For example, LDI-MS is suitable for detecting small drug molecules by photoionization, MALDI-MS and LA-ESI-MS are suitable for molecules that are easily protonated and LA-ICP-MS is used for samples in which the relevant analytes are metal elements. However, because of the optical diffraction limit and lens aberration, it is still difficult to obtain sample information at subcellular resolution for laser-based MSI[23].

It is recognized that the spatial resolution of MSI directly depends on the sampling spot size. Until now, the design of laser-based ion sources for high-resolution imaging has been specialized and expensive, which has limited nanoscale MSI applications to life science, nanomaterials and cellular biology. Here, we introduce an experimental protocol for a universal and economical laser-based nanoscale sampling method by using a microlensed fiber, which can be easily combined with different MSI techniques for the imaging of tissue sections and single cells. These microlenses can be cheaply and easily fabricated by using the approach described in this protocol.

### Development of the protocol

We have developed a strategy for replacing the traditional laser path system with a microlensed fiber. Without changing the original ionization mechanism, the microlensed fiber is combined with multiple MSI platforms to achieve subcellular spatial resolution, as demonstrated previously for LDI-MSI, MALDI-MSI, LA-ICP-MSI and LA-ESI-MSI[22,24–27]. By changing the laser energy and the distance between the fiber tip and sample surface, we are able to obtain sampling spots ranging from 350 nm to 10 μm in diameter. MSI of a standard grid sample demonstrated that a microlensed fiber can achieve ~300-nm spatial resolution under optimal conditions[24].

We have applied the microlensed fiber to biological tissue imaging and single-cell imaging[22,24,26,27]. For animal tissue imaging, we are able to visualize the distribution of three photosensitive drugs, cobalt tetrasulfonate phthalocyanine (CoTsPc), copper phthalocyanine (CuPc) and zinc phthalocyanine (ZnPc), in a small-intestine slice from a mouse[26]. The nanoscale-resolution MS images help to reveal the vital function of the epithelium and blood capillaries of intestinal villi in the absorption and transportation of drugs. For plant tissue imaging, we are able to identify the location of different metabolites of a parsnip root sample[22]. The boundaries between xylem, phloem, cambium and cortex can be easily distinguished. In addition, we achieved single-cell imaging of multiple drugs and nanomaterials at the organelle level. With the high-resolution MSI platform, traces of acriflavine and azure B (two anti-inflammatory drugs) are found in the cytoplasm and nucleolus of HeLa cells[24]. By comparing with the fluorescence image of the lysosome and nucleus dye (DND-99 and Hoechst-33342), the distributions of superparamagnetic iron oxide and gold nanorods are shown to be in the lysosomes of cells, which indicates that the nanomaterials are ingested by the cells through endocytosis. In addition, the dynamic process of anticancer drug molecules released from nanoparticle carriers in lysosomes and entering the nucleus, finally leading to apoptosis of cancer cells, can be clearly captured by monitoring the physical feature of cell shrinkage.

### Applications of the method

By sampling smaller areas inside each pixel, subcellular-resolution MSI with a microlensed fiber allows better-resolution images, which can help to identify chemical diversities and details and provide an opportunity for diversiform fields. For single-cell analysis, the traditional MS

method refers to stochastic average values masked by bulk measurements, resulting in a loss of information related to intercellular chemical heterogeneities in large cell populations. Our protocol makes it possible to understand chemical differences between organelles. The distribution of metabolites can be visualized within a single cell or biological tissue section with different laser-based MSI techniques. The monitoring of drug uptake, transfer, location and metabolism provides valuable indicators in biological and clinical medicine research, while our technique has been proven to be well suited for extending these studies down to the subcellular level. For many laboratories, commercial MSI platforms with laser sources are already available. It is suggested that existing laser-based MSI platforms can achieve breakthroughs in spatial resolution by introducing a microlensed fiber as part of the laser ionization setup.

### Development of the microlensed fiber

The principle of using a microlensed fiber is a refinement of the traditional laser-focusing approach. The 'microlens' on the tip of the fiber focuses the laser light on a smaller point of the sample. The lens has a defined radius of curvature and is fabricated by using a self-made fiber-grinding machine. In our work, the lens fabrication was done in collaboration with Chuxing Optical Fiber Application Technology.

The choice of the fiber depends on the experimental requirements. For MSI experiments, the wavelength required for ablation or desorption is one of the most important factors.

- Because of the mechanism of photoionization, LDI-MSI experiments usually require visible or UV lasers, which have a higher photon energy[28].
- In MALDI-MSI, the wavelength of the laser needs to be selected in accordance with the absorption wavelength of the matrix molecules[29].
- For LA-ICP-MSI, the laser is mainly used for the ablation and vaporization of the sample, while a matrix effect and fractionation effect would be observed with a different wavelength[30,31].

To achieve the highest laser transmission efficiency, the transmission wavelength of the fiber should be consistent with the laser wavelength. In addition, the use of a pure silica fiber is recommended to avoid photo-darkening, instead of an elemental doped fiber while using UV laser light. A single-mode fiber has a better focusing effect but less light throughput. Before processing the microlensed fiber, a single-mode fiber or multi-mode fiber should be chosen according to the experimental needs. In this protocol, we provide the processing parameters of one single-mode fiber (core diameter of 2.5 µm; F-SM-300-SC, Newport) and one multi-mode fiber (core diameter of 16 µm; FM SI-2-ULL, Yangtze Optical Fiber Company) that have been used in our previous studies. Both of these two fibers have a coating of 250 µm and a cladding of 125 µm in diameter.

Figure 1a presents a schematic diagram of how the microlensed fiber is fabricated. First, use a fiber-stripping tool to remove the outer coating. The exposed cladding length is ~3 mm. Then, use a fiber-grinding machine to make the microlens on the fiber tip. The radius of curvature of the microlens is the only parameter considered during the process; the radii are 4.5 and 10 µm for the single-mode fiber and multi-mode fiber, respectively. Figure 1b shows a photograph of a microlensed fiber, which has a length of 1 m. Figure 1c is the microscopic image of the microlens on the fiber tip in Fig. 1b.

As shown in Fig. 1d, similar to the focusing principle of a flat convex lens, the laser beam emitted from the microlensed fiber is focused by the curved surface. The equation of microlens focusing is:

$$f = \frac{1}{(n-1)\left(\frac{1}{R_1} - \frac{1}{R_2}\right)},$$

where $n$ represents the refractive index of the laser wavelength, and $R_1$ and $R_2$ ($+\infty$) represent the radii of curvature on both sides of the microlens, respectively. Figure 1e shows the schematic diagram of the microlensed fiber beam path. The output beam from the laser is coupled into the microlensed fiber with a lens. Because it is difficult to detect the real-time output laser energy from the microlensed fiber during MSI, we use a beam splitter (50:50) to monitor the input laser energy. Then, the actual laser energy applied on the sample can be known by calculating with the input energy (on the power meter) and fiber coupling efficiency (Supplementary Fig. 1).

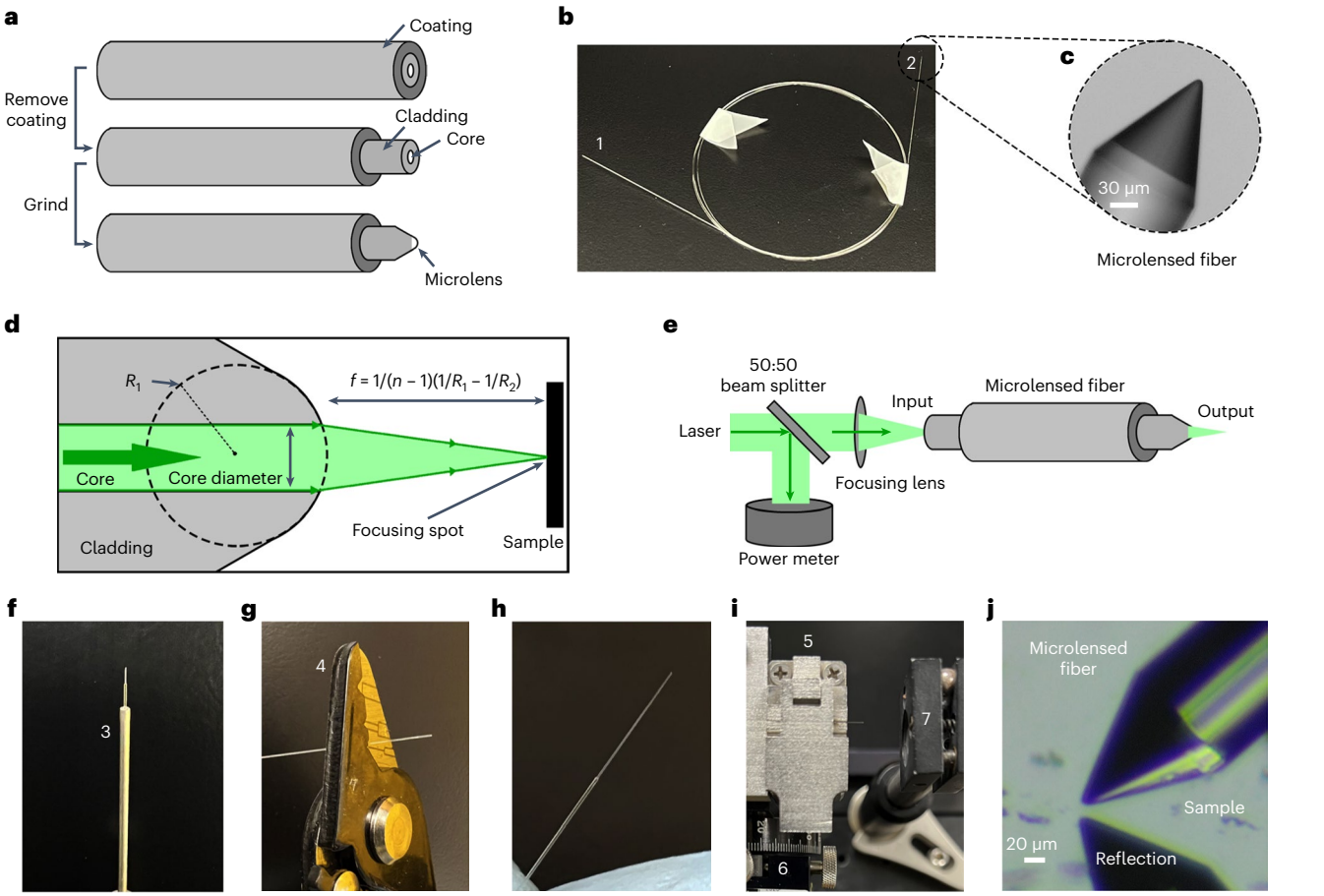


**Fig. 1 | Development of the microlensed fiber and its positioning. a**, Schematic of the manufacturing process of the microlensed fiber. **b**, Photograph of a microlensed fiber. The length of the fiber can be customized according to the laser path. The fiber shown in the photo is 1 meter long. 1: rear end of the microlensed fiber. 2: microlens tip. **c**, Microscopic image of the microlens tip. **d**, Focusing principle of the microlensed fiber. **e**, Schematic diagram of the beam path of using a microlensd fiber for high-resolution MSI experiments. **f**, Microlensed fiber pipe. 3: stainless-steel drive pipe. **g**, Using a fiber-stripping tool to remove the coating at the end. 4: fiber stripping tool. **h**, The rear end of the fiber after processing with a fiber cleaver. **i**, Laser coupling into the microlensed fiber with a lens. 5: fiber clamp. 6: 3D positioner. 7: focusing lens. **j**, Real-time observation of the microlensed fiber sample area with a CCD microscope. Images in **c** and **d** adapted with permission from ref. 24, Wiley.

To fix the microlens tip of the fiber, we insert the fiber into a stainless-steel pipe, which has an inner diameter of 300 μm and an outer diameter of 1 mm (Fig. 1f). While inserting the fiber, we recommend that insertion takes place from the rear end to avoid abrasion of the microlens. UV-curable adhesive can be used to bond together the fiber and the pipe. For the highest coupling efficiency of the laser, we use a fiber-stripping tool to remove the coating at the end (Fig. 1g). Then, we use a fiber cleaver to make a flat tip (Fig. 1h). The flat tip of the fiber is fixed with a fiber clamp, which is mounted on a 3D positioner. As shown in Fig. 1i, the laser is coupled into the fiber with a lens ($f$ = 20 mm). During the laser coupling procedure, use the laser energy meter to measure the energy output from the microlensed fiber. The highest output energy can be obtained by adjusting the 3D positioner. A charge-coupled device (CCD) camera with a 0.7–4.5× microscopic lens is used to monitor the microlensed fiber and sample area (Fig. 1j).

## Experimental design

### Fitting the microlensed fiber to different mass spectrometers

There are various commercially available laser-based MSI platforms, and the procedures for performing MSI by using each of these will be different. The MSI process is not the topic of this

protocol and is expected to be largely unchanged by the introduction of the microlensed fiber. The Procedure of this protocol focuses on the setup of the microlensed fiber device and how it can be integrated into MSI platforms to achieve subcellular spatial resolution. Although it could be applied to many platforms, we provide detailed instructions for three that we have used in our previous research.

*LDI-MSI platform with a time-of-flight (TOF) mass analyzer: Step 11A*. In traditional approaches, the laser is focused from outside of the mass spectrometer through a lens and applied into the sample area through a viewing window. The long working distance allows the laser spot size to only reach ~100 µm. In our protocol, we coupled the laser into the microlensed fiber, transmitting and focusing the laser to the sample surface by the microlens. A home-built TOF-MS is combined with the microlensed fiber for the nanoscale MSI experiment.

Figure 2a presents a schematic diagram of the imaging platform. An image of the LDI-MSI platform is shown in Supplementary Fig. 2. Both the ion source and the TOF mass analyzer are placed in the same vacuum chamber (~$8 \times 10^{-5}$ Pa) so that ion losses caused by transmission can be reduced to a minimum. Ions are produced by the high-power-density laser over the sample surface and pulled into the acceleration region by the pulsed electric field. The energy dispersal of the ions can be focused by a time-lag focusing technique and a double-stage reflectron, facilitating improved mass spectral resolution. Finally, the ions arrive at the detector assembled with two microchannel plates. A digital oscilloscope (42MXs, LeCroy) was used to record the mass spectral signals.

The imaging process was controlled by self-written software by LabVIEW (see the panel in Supplementary Fig. 3). We fix the fiber into the ion source region by inserting it into a bent stainless-steel tube, which is mounted on a one-dimensional micropositioner (SLC-1720, SmarAct). Thus, the distance between the fiber tip and sample surface can be controlled to find the best focal length, which can be observed through a CCD camera. The fiber entered the vacuum chamber through a vacuum feedthrough. A typical imaging process is shown in Supplementary Video 1.

*LA-ICP-MSI platform with a commercial ICP-MS (Series 7700, Agilent Technology): Step 11B*. Figure 2b is a schematic diagram of the LA-ICP-MSI platform with a microlensed fiber, which mainly consists of three parts: the microlensed fiber (laser system), the sample ablation chamber, and the ICP-MS.

The ablation chamber is made of fused quartz. Supplementary Fig. 4 shows the MSI platform and the ablation chamber with its three-way structure. The three branch tubes are designed for the microlensed fiber, sample stage and capillary that transported the aerosols. The inner diameter of each quartz tube is 3 mm. The ablation chamber was fixed to the sample stage, while the scanning process was realized by moving the microlensed fiber. By stretching into a stainless-steel pipe, the fiber was fixed on a 3D micropositioner (SLC-1720, SmarAct), which controlled the fiber-sample distance (through the *z* axis) and the ablation area (through the *xy* axes). The ablation chamber and fiber pipe were connected by a flexible silicone tube. In that way, the fiber was able to move freely over the sample surface while keeping the airtightness of the ablation chamber. The generated aerosols flew from the ablation chamber to the ICP torch with the carrier gas. Spatial distributions of multiple elements could be obtained by monitoring different mass-to-charge ratios (*m/z*) with the mass spectrometer. The microlensed fiber and the sample surface can be observed in real time by the CCD camera (Supplementary Fig. 5).

*LA-ESI-MSI platform with a commercial Orbitrap MS (Velos Pro, Thermo Fisher): Step 11C*. As an ambient MSI technique, LA-ESI-MSI was introduced recently by the Vertes group[21,32,33]. In the published research, LA-ESI-MSI is mainly performed by focusing the laser with a lens or by using a chemical etched fiber, which could achieve a spatial resolution from 30 to 100 µm. In this protocol, we provide detailed information about the LA-ESI-MSI platform with a microlensed fiber, which can achieve 5-µm spatial resolution. The charged droplets are generated by a self-assembled nanoelectrospray ionization (nanoESI) emitter. Analytes on the sample surface

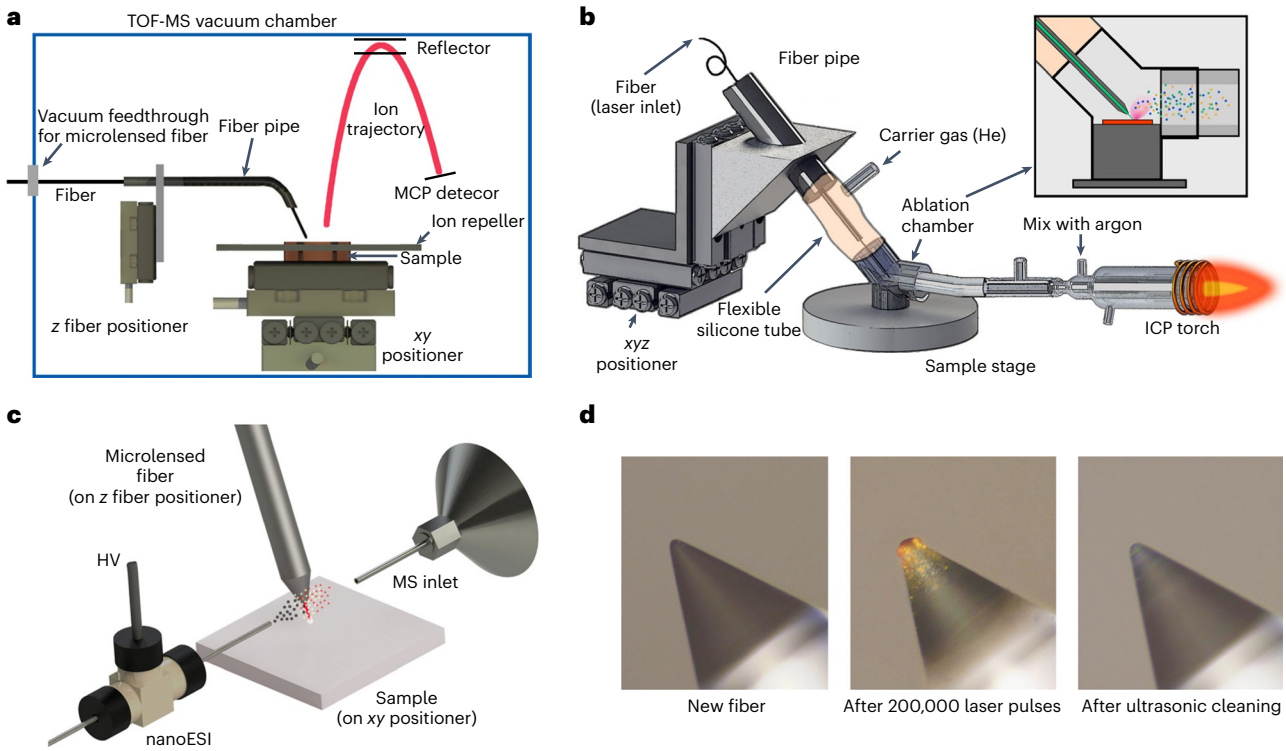


**Fig. 2 | Schematics of different types of laser-based MSI platforms with the microlensed fiber. a**, LDI-TOF-MSI platform. **b**, LA-ICP-MSI platform. **c**, LA-ESI-MSI platform. **d**, The lifetime of the microlensed fiber. MCP, microchannel plate; nanoESI, nanoelectrospray ionization. Image in **b** adapted with permission from ref. 26, American Chemical Society. Images in **c** and **e**–**j** reproduced with permission from ref. 22, American Chemical Society. Image in **d** adapted with permission from ref. 24, Wiley.

are first desorbed mostly in the neutral form by the laser applied with the microlensed fiber. After colliding with charged droplets from the electrospray source, analytes are ionized and transmitted into the heated inlet of a mass spectrometer, and the resulting ions are sorted by their $m/z$. The X-distance (from the sampling spot to the electrospray emitter in the horizontal direction) and Z-distance (from the sample surface to the mass spectrometer inlet in the vertical direction) are accurately optimized to 0.5 and 2.0 mm, respectively. A photo of the experimental setup is shown in Supplementary Fig. 6.

## Lifetime of the fiber

The lifetime of the microlensed fiber is an important consideration because of the long hours of laser sampling during MSI. Our research result shows that, under the premise of reasonable use, the lifetime of the fiber can reach millions of laser pulses. Reasonable use here means that there is no damage to the fiber tip from physical damage and no input laser of excessively high energy. Because the fiber is usually only a few tens of microns away from the sample, sample deposition on the fiber tip is unavoidable. As shown in Fig. 2d, after 200,000 laser ablations on a proflavine tablet sample, proflavine molecules were deposited on the surface of the fiber tip. When we evaluated the lifetime of the microlensed fiber on the proflavine tablet sample, we monitored the signal intensity in the meantime (Supplementary Fig. 7). Without changing the laser energy, we saw that the signal intensity of proflavine did not have a big decrease after 200,000 laser shots. This might have been because the contamination mainly occurred around the tip of the fiber and did not affect the output of the laser. The main factor of when a fiber needs to be cleaned is a significant reduction in signal intensity. Results showed that we did not need to clean or change the fiber after 200,000 laser shots. To save the life of the laser, we did not perform endless evaluation of the fiber lifetime. If cleaning is necessary, the microlensed

fiber can work normally after ultrasonic cleaning with ethyl alcohol. The ultrasonic cleaner that we used is a 400 W machine with a 40-kHz frequency (CR-060S, ChunRain Technology). When changing the cleaner power to 900 W (CR-180ST, ChunRain Technology), we did not observe a destructive effect on the fiber in the ultrasonic cleaning step.

## Spatial resolution

For most imaging techniques, high spatial resolution is highly valued. For laser-based MSI, data acquisition requires the use of a laser to scan the sample, pixel by pixel. That means, for the same imaging area, higher resolution requires longer times. In addition, the smaller sampling spot requires higher sensitivity of the mass spectrometer. With the microlensed fiber, we are able to achieve a spatial resolution from 300 nm to 10 µm. As shown in Fig. 3a, by changing the applied laser energy and the distance between the fiber tip and the sample surface, different sizes of sampling craters can be obtained, which demonstrates that the microlensed fiber technique is able to be used in different applications. Figure 3b shows the optical image of a standard copper grid sample, which was used for the representation of the spatial resolution of the MSI with a microlensed fiber. The spatial resolution is normally defined by the distance between 20% and 80% signal-intensity change of a line-scan profile containing a sharp edge. During the scanning of the copper grid, the size of the sampling crater is set as ~350 nm. The frequency of the laser and the moving speed of the sample are set as 10 Hz and 3 µm/s, respectively; the distance between the neighboring sampling spots is 300 nm. Figure 3c shows the signal intensity profile of $Cu^+$ of the outlined region of Fig. 3b. By choosing two sharp edges, the best spatial resolution is revealed to be ~300 nm. We also investigated the sampling craters on an adherent cell. Results showed that the mean ± s.d. diameter of the sampling spots on a HeLa cell was 350 ± 40 nm, which offered the potential of this method for single-cell imaging (Supplementary Fig. 8). This result was achieved by using the LDI-MSI platform[24].

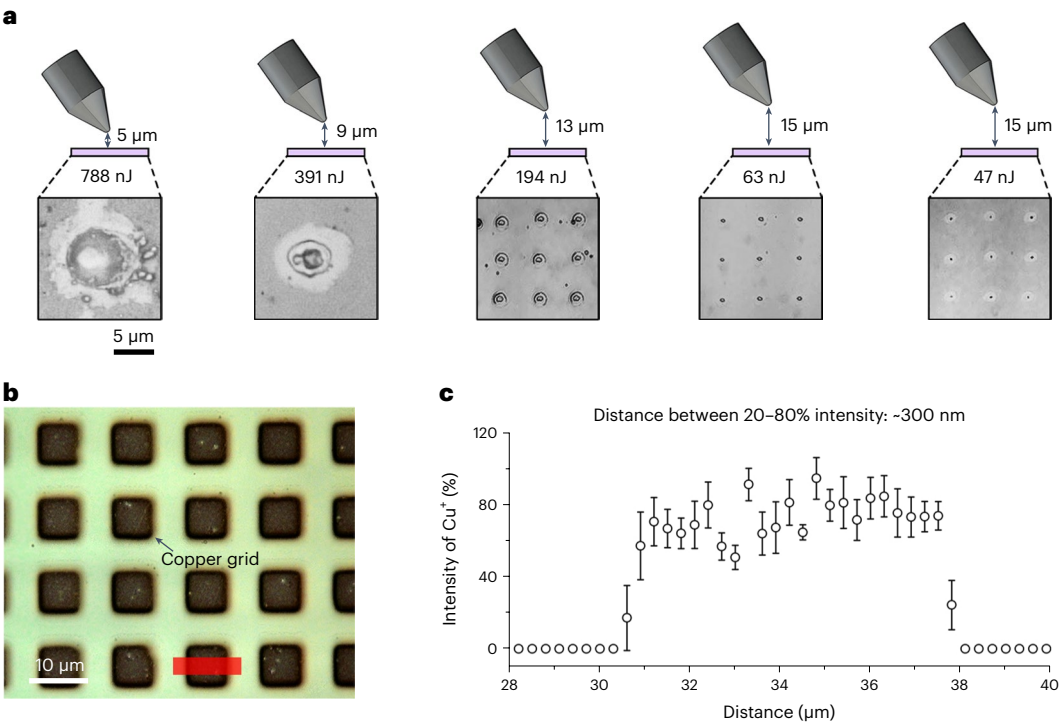


**Fig. 3 | Spatial resolution of the MSI with a microlensed fiber. a**, Sampling craters of different sizes obtained by changing the applied laser energy and the distance between the fiber tip and sample surface. **b**, The optical image of a standard copper grid sample used for the representation of the spatial resolution of the MSI with a microlensed fiber. **c**, Signal intensity profile of $Cu^+$ of the marked region in **b**, which indicates that a spatial resolution of ~300 nm has been achieved. Error bars represent the standard deviation of the signal intensities. Images in **a** adapted with permission from ref. 26, American Chemical Society. Images in **b** and **c** adapted with permission from ref. 24, Wiley.

## Comparison with other methods

There are several types of commercially available MSI techniques depending on the ion source, such as secondary ion MS (SIMS)[34], which uses a focused ion beam for sampling; desorption ionization electrospray ionization (DESI) MS[35–37], which uses a spray of charged droplets for sampling; and laser-based MS.

The approach described in this protocol is very useful for acquiring high-resolution information at the single-cell level. There are, however, many applications in which lower-resolution methods are more useful; for example, if it is necessary to image a sample with a large area, and it is sufficient to determine the approximate distribution, high-resolution imaging will cost too much time. Other approaches to high-resolution MSI are described here.

Nanoscale SIMS has been proven useful for MSI at a resolution of dozens of nanometers but can obtain only elemental images[38,39]. TOF-SIMS is acknowledged for single-cell imaging at a lateral resolution of hundreds of nanometers but is always accompanied by the appearance of complex fragments and additives[34,40]. The spatial resolution of DESI-MSI is ~100–200 µm, which limits its applications in microscale imaging[35,41]. Recently, the Laskin group has developed a novel technique named 'nano-DESI', which is able to achieve a spatial resolution of 10 µm[42]. However, it appears at present to be unable to meet the requirements for single-cell imaging.

As mentioned above, laser sampling can be combined with different ion sources and can be used to analyze different sample types. Recent decades have witnessed great improvements in the lateral resolution of laser-based MS from microscale to nanoscale. To date, a spatial resolution of 1.4 µm can be achieved by atmospheric pressure MALDI-MSI with a home-built laser-focusing device[43]. In addition, by focusing the laser from the back of the sample, the transmission geometry MALDI-MSI is able to achieve submicron spatial resolution[44–46]. Currently, these techniques have been applied only to MALDI-MSI. With near-field optical techniques, spatial resolutions beyond the diffraction limit can be achieved[47–49]. By reducing the laser wavelength, vacuum ultraviolet[50] and extreme UV[51] laser ionization MSI have been shown to reach a nanoscale resolution down to 300 nm with the LDI-MSI platform. However, the complex laser system and the high cost limit their applications. An ablation tube cell, based on a constant laminar flow and a well-controlled delivery of ablated aerosol into the ICP torch, was able to improve spatial resolution to the subcellular level (~1 µm)[19]. By coupling this ablation chamber to a TOF ICP-MS (mass cytometer), proteins labeled with rare earth elements could be visualized for biological samples[52].

The protocol of the microlensed fiber for laser-based imaging that we describe here has been verified to be a universal technique for multiple applications. The existing laser-based MSI platforms can achieve breakthroughs in spatial resolution by introducing a microlensed fiber. It is worth mentioning that the microlensed fiber can achieve high-resolution MALDI-MSI by coupling with a UV laser (such as a 355-nm nanosecond laser). As an untargeted imaging approach, MALDI-MS offers opportunities for the visualization of lipids, fatty acids and more metabolites in a biological sample. Supplementary Fig. 9 shows a preliminary result of combining MALDI-MS with the microlensed fiber. Particularly, by combining with post-ionization techniques, such as laser post-ionization[47] and dielectric barrier discharge ionization[53,54], the ionization efficiency and signal intensity can be further improved even though the sampling spots are small.

## Limitations

During our experiments, the time spent depends mainly on the size of the sampling area. The laser pulse rate used in the current experiment is 10–20 Hz. A higher-pulse-rate laser and faster acquisition rate of the mass spectrometer could effectively reduce the time required for the experiment, but with added costs. Another limitation is that, compared with traditional laser-focusing methods, the MSI technique using a microlensed fiber has a low tolerance for the height fluctuation of the sample. During the experiment, the distance between the fiber tip and the sample surface should be several microns; a large height fluctuation of sample can cause collisions between the fiber and the surface. In addition, the focusing spot size changes when

the distance between the sample and the fiber changes greatly. Our result indicates that signal intensity and crater size do not change significantly within plus or minus one micron of the focal point (Supplementary Fig. 10), implying that this technique is suitable to perform nanoscale MSI experiments on samples regardless of height fluctuations within two microns, such as a tissue slice and adherent cells.

Analyzing a smaller sampling spot means that less material reaches the detector, making it more difficult to detect compounds that are present at lower concentrations. To reduce this problem, detection sensitivity and ionization efficiency can potentially be improved by using certain post-ionization methods, such as laser post-ionization and dielectric barrier discharge post-ionization.

This protocol requires a sample stage that can be moved in very small increments. Most commercially available MSI platforms do not use a piezo-driven sample stage. The more common leadscrew and stepping-motor based stages are limited to a step size of 1–5 µm. To achieve nanoscale MSI, it is therefore often necessary to change the sample stage.

## Materials

### Equipment

▲ **CRITICAL** Two options are listed for the silica fiber: single mode and multi mode.

- Single-mode pure silica fiber (core diameter: 2.5 µm; F-SM-300-SC, Newport)
- Multi-mode pure silica fiber (core diameter: 16 µm; FM SI-2-ULL, Yangtze Optical Fiber)
  ▲ **CRITICAL** The fiber type needs to be suitable for the wavelength of the laser.
- Three-hole fiber stripper (Thorlabs, part no. FTS4)
- Optical fiber cleaver (Sumitomo Electric Industries, cat. no. FC-6S)
- Fiber grinder (ULTRAPOL, ULTRA TEC Manufacturing)
- Fiber clamp (SOFN Instruments, cat. no. 7MFP06)
- Fiber pipe (i.d.: 0.5 mm; o.d.: 1 mm)
- Fused silica focusing lens (no coating, $f$ = 20 mm; Hengyang Guangxue, cat. no. GLH21-012-020)
- UV air-spaced achromatic doublet lens (anti-reflection coating: 245–400 nm, $f$ = 100 mm; Thorlabs, cat. no. ACA254-100-UV)
- Ø1/2-inch precision kinematic mirror mount (Thorlabs, cat. no. KS05)
- Ø1-inch precision kinematic mirror kount (Thorlabs, cat. no. KS1)
- Ø1-inch Nd:YAG mirror (1,047–1,064 nm, 0–45°; Thorlabs, cat. no. NB1-K14)
- Ø1-inch Nd:YAG mirror (524–532 nm, 0–45°; Thorlabs, cat. no. NB1-K12)
- Ø1-inch Nd:YAG mirror (349–355 nm, 0–45°; Thorlabs, cat. no. NB1-K08)
- Ø1-inch Nd:YAG mirror (262–266 nm, 0–45°; Thorlabs, cat. no. NB1-K04)
- High-precision linear stage (Zolix Instruments, cat. no. SK13A-40SR)
- Linear stage (Zolix Instruments, cat. no. AK25A-8020SR)
- Linear stage (Zolix Instruments, cat. no. AK25-8020LZ)
- High-precision linear stage (Zolix Instruments, cat. no. SK25A-65SL)
- XYZ translation stage (Thorlabs, cat. no. LX30)
- XYZ translation stage with standard micrometers (Thorlabs, PT3)
- CCD camera (Ruixian Optics Technology)
- 0.7–4.5× microscope for CCD camera (Sannuo Electronic Technology, cat. no. XDC-10A)
- 0.5× microscope objective (working distance = 165 mm; Sannuo Electronic Technology)
- 1.5× microscope objective (working distance = 45 mm; Sannuo Electronic Technology)
- Microscope stand (Shanghai Meimei Metering Electricity Technology, cat. no. STL6C)
- Kimwipes (Kimberly-Clark Professional, cat. no. 34155)
- Nanosecond laser (Continuum Electro-Optics, Minilite II)
- Femtosecond laser (Amplitude Systèmes, s-Pulse-HP)
- Nanosecond laser (Spectra-Physics, cat. no. DCR-11)
- Barium metaborate crystal for UV output of femtosecond laser (Core Optronics)

- Laser energy meter (MKS, Ophir Vega)
- Linear micropositioner for sampling moving (SmarAct, cat. no. SLC-1720)
- 'Three-way' ablation chamber (made by quartz tube, with i.d. of 3 mm and o.d. of 4 mm; a blueprint of the chamber is provided in Supplementary Fig. 11)
- Ultrasonic cleaner (400 and 900 W; ChunRain Technology, cat. nos. CR-060S and CR-180ST, respectively)
- Flexible silicone tube for carrier gas
- Gas flowmeter (0–3 liters/min)
- Home-built TOF mass spectrometer (Wei Hang's laboratory, Xiamen University, China)
- ICP-MS (Agilent Technology, Series 7700)
- Orbitrap mass spectrometer (Thermo Fisher, Velos Pro)
- Delayed pulse generator (Quantum Composers, model 9514)
- Flexible fused-silica capillary (i.d.: 75 µm; o.d.: 375 µm; Polymicro Technologies)
- MicroTee PEEK (360 µm; IDEX Health & Science)
- MicroTight sleeve, green (0.025-inch o.d. × 0.0155-inch i.d.; Idex Health & Science)
- Cleaving stone (1 inch × 1 inch; Polymicro Technologies)
- Ceramic heater (o.d.: 5 mm; i.d.: 3 mm; Xinxinshiji)
- 2D micropositioner (Micro-Stage Systems, Mad City Labs)
- Continuous beam attenuator for femtosecond laser (CVI Laser Optics, cat. no. ABSO-6.35)
- 500-µl syringe (Hamilton, model 1750 RN)
- Syringe pump (Cole-Parmer, model 110)
- Microtome (Leica Microsystems, cat. no. RM2235)
- Freezing microtome (Leica Microsystems, cat. no. CM1590)
- Confocal laser scanning microscope (Leica Microsystems, cat. no. SP8-STED 3X)
- Magnetron sputtering system (Denton Vacuum, Explorer 14)
- Copper grid (Gilder Grids, cat. no. G2000HS-C3)

### Biological materials

Some biological materials can be analyzed by using the methods described in the Procedure. In the Anticipated results section, we have included results for the detection of drug distribution in mouse intestines, metabolites in parsnip roots and nanomaterial/drug distribution in HeLa cells. Here, we provide the detailed sample preparation procedures corresponding to what we report in Anticipated results.

- *Mouse intestines*. The 5-week-old female BALB/c mice used in this experiment were provided by Xiamen University Laboratory Animal Center. All animal experiments were conducted with the approval of the animal ethics and use committee of Xiamen University. Mice were housed in controlled light (12-h light/dark cycle), temperature and humidity conditions with free access to food and water. CuPc, ZnPc and CoTsPc were co-dissolved in deionized water containing 20% (vol/vol) dimethyl sulfoxide.
  - After 12 h of fasting, mice were given a single dose of the mixed drugs (100 mg/kg body weight, intragastric).
  - One hour later, the mice were suffocated in $CO_2$.

  A conventional paraffin method was used for tissue section preparation as follows:
  - Fresh small-intestine samples were soaked in formalin (4% (vol/vol) methanal) solution for 24 h[26]. Then, the samples were wrapped in gauze and rinsed under flowing pure water for 24 h.
  - After being washed, the samples were then soaked in 50%, 70%, 85%, 95% and 100% (vol/vol) ethanol for 1 h successively[26].
  - The tissue was placed in a mixed solution of ethanol and xylene (volume ratio of 1:1) for 2 h, then in xylene for 2 h and finally in a mixed solution of xylene and paraffin (volume ratio of 1:1) for 2 h at 60 °C. The sample was fixed in a paraffin chunk by using a paraffin-embedding machine (Leica Microsystems, Arcadia).
  - Tissue sections with a thickness of 10 µm were obtained with a microtome (Leica Microsystems, cat. no. RM2235).

- Then, the sections were dewaxed by placing the section in 100%, 90%, 70%, 50% and 30% (vol/vol) xylene (ethanol solution) for 10 min successively, soaking the section in ethanol and water for 5 min in order[26].
- Finally, the section was mounted in the ablation chamber.

For this protocol, mice were chosen because they are a readily available laboratory animal for sample preparation. The sex of mice does not affect the suitability of the samples for experiments involving laser ablation and MS imaging.

▲ **CAUTION** Any experiments involving live mice must conform to relevant institutional and national regulations.

- *Parsnip roots*. We chose parsnip root because it has a well-defined architecture, and we can get it cheaply from the market. The parsnip root was cut into 100-μm-thick slices by a freezing microtome (Thermo Scientific, cat. no. HM525 NX) without any treatment. The section was then put on a glass slide for further imaging.
- *HeLa cells*. We chose HeLa because it is a commonly studied adherent cell line. HeLa cells are grown in DMEM (HyClone) supplemented with 10% (vol/vol) FBS, 1% (vol/vol) penicillin (Gibco) and 1% (vol/vol) streptomycin (Solarbio Life Sciences, Beijing, China)[47].
  - Seed the cells into 150-mm Falcon culture dishes and maintain them by adding fresh medium every 2–3 d.
  - Rinse the quartz plates in HPLC-grade water and ethanol to sterilize.
  - Place the quartz wafers in a six-well plate, seed the cells into the wells at a cell density of $1 \times 10^3$ to $1 \times 10^4$ cells/well (the number of cells is dependent on the desired coverage) and allow them to grow for 24 h at constant conditions of 37 °C and 5% $CO_2$.
  - Incubate the adhered cells in the six-well plate with the desired concentrations of drugs or nanoparticles for several hours. The culture time and drug concentration depend on the experimental plan.

For CLSM imaging:

- Incubate the cells with Lyso-Tracker Red DND-99 and nuclear dye Hoechst 33342 for 1 h.
- Wash the quartz plates containing cells three times in PBS solution and image by using a laser confocal microscope.

For MSI:

- Rinse the quartz wafers with adherent cells three times with 150 mM ammonium acetate at a pH of 7.4 to remove undesired salts after paraformaldehyde fixation.
- Before the cryofixation process, wipe the edges of the quartz wafers with a Kimwipe tissue for 2 s to remove excess medium.
- Freeze the quartz wafers in liquid isopentane that was precooled by liquid $N_2$ and transfer immediately into the vacuum of a freeze drier at a temperature of −65 °C.
- After freeze-drying for 2 h, mount the cells adhered on quartz wafers onto the sample stage for the MSI measurements.

### Other analyte materials

- In addition to biological samples, other types of materials that have a flat surface and micro-structure could also benefit from high-resolution MSI with a microlensed fiber; for example, we have shown that the profile of a core–shell microsphere can be visualized by LDI-MSI[25].

### Reagents

- Surgipath paraplast (high melt; Leica Biosystems)
- HyClone DMEM (Sigma-Aldrich)
- Penicillin-streptomycin-glutamine (Gibco Thermo Fisher Scientific)
- FBS (Gibco Thermo Fisher Scientific)
- Trypsin 1:250 (Beijing Solarbio Science & Technology)
- LysoTracker Red (Bioluminor Bio-Technology, cat. no. DND-99)
- Hoechst 33342 solution (Thermo Fisher Scientific)
- 16% Paraformaldehyde solution (Thermo Fisher Scientific)

## Procedure

▲ **CAUTION** The optical fiber used in this protocol is sharp. Any operation with the fiber should be done only while wearing nitrile powder-free gloves, a laboratory coat and safety glasses. All laser operations should follow safety rules. Laser-protection glasses are required while doing the experiment.

### Fabrication of the microlensed fiber

● **TIMING 30 min**

▲ **CRITICAL** The design of the microlensed fiber is finished by our laboratory, while the fabrication is in collaboration with Chuxing Optical Fiber Application Technology. The same microlensed fiber that we use in this protocol is commercially available from the company's website (http://www.cxfiber.com/). The radius of curvature of the fiber is the key parameter for high-resolution MSI.

1. Preparation before fiber grinding. The commercially available optical fibers are usually sold wrapped around fiber spools. The length of the fiber depends on the design of the experimental laser beam path. In this protocol, the length of all fibers is set as 1 m.
   - Cut 1 m of fiber with the fiber cleaver.
   - Remove 3 mm of the outer coating of one end of the fiber with the three-hole fiber stripper. Notice that the diameter of the coating of the fiber used in this protocol is 250 µm. Use the smallest hole on the three-hole fiber stripper to remove the outer coating.
   - Use Kimwipes to carefully clean the tip of the fiber.

     ▲ **CAUTION** The fiber is very sharp and is able to puncture gloves. You should be very careful while handling a fiber.
2. Fiber grinding
   - Use the fiber holder on the grinding machine to tighten the end of the fiber from which the outer coating has been removed.
   - Adjust the distance between the fiber tip and the grinding disc to 1–2 mm.
   - Input the required radius of curvature (4.5 µm for F-SM-300-SC fiber, 10 µm for FM SI-2-ULL fiber) to the fiber-grinding machine and then wait for the automatic grinding fabrication.

     ▲ **CAUTION** Keep your hands away from the grinding disc while the grinder is working.
3. Remove the microlensed fiber from the grinding machine. Clean the microlens tip with ethyl alcohol in an ultrasonic cleaner for 5 min.

   ▲ **CRITICAL** This step needs to be done carefully. Even a slight bump can cause damage to the fiber tip.
4. Check the quality of the laser beam output from the microlens with a laser beam quality analyzer.
5. Coil the fiber and secure it with tape for easy placement in the fiber box.

   ▲ **CRITICAL STEP** This step should be performed carefully. Even a slight bump can cause damage to the fiber tip.

### Installation of the laser sampling device with a microlensed fiber

● **TIMING 20 min**

▲ **CRITICAL** Fig. 1f–i shows the installation process of the sampling device with a microlensed fiber. With this setup, the microlensed fiber can be combined with different types of laser-based MSI platforms. If you are using an LDI-MSI platform, refer to Step 11A(ii) before performing Step 9.

6. Take the microlensed fiber (Fig. 1b) out of the fiber box. Insert the fiber into the stainless-steel fiber drive pipe from the rear end.

   ▲ **CRITICAL STEP** This step should be done carefully. Even a slight bump can cause damage to the fiber tip.
7. Control the distance between the microlens tip and the front section of the fiber pipe; this distance should be 3–5 mm. Use UV-curable glue to secure where the fiber contacts the front section of the pipe.

▲ **CAUTION** While using UV light, avoid direct light sources to the eyes.

▲ **CRITICAL STEP** UV-curable glue should be used carefully. Too much glue can damage the tip of the microlensed fiber.

8. Remove 5 mm of the outer coating of the rear end of the microlensed fiber by using a fiber stripper. Use the fiber cleaver to get a flat surface for the coupling of the laser (Fig. 1g,h).
9. Put the rear end of the fiber (flat surface) into the fiber clamp. Focus the laser on the surface of the fiber with an objective lens (Fig. 1i). Notice that the beam path is not the topic of this protocol. The laser collimation, generation of different wavelengths and laser path design are not included in this protocol. As a typical example, just use an objective lens ($f$ = 20 mm) to focus the laser (532 nm) into the rear end of the fiber.

◆ **TROUBLESHOOTING**

10. Put the laser energy meter in front of the microlensed fiber. Carefully adjust the 3D positioner that holds the fiber clamp to achieve the highest coupling efficiency; i. e., optimize the output laser energy from the microlensed fiber to its highest value.

▲ **CRITICAL STEP** Wear laser-protection glasses. Carefully control the input laser energy. A high-energy laser will cause damage to the back end of the fiber. After optimizing the coupling of the laser, avoid moving the laser path or fiber clamp.

◆ **TROUBLESHOOTING**

11. Combine the microlensed fiber device with your MSI platform. The steps to do this depend on which platform is used. We have included example procedures for our LDI-MSI (option A), LA-ICP-MSI (option B) and LA-ESI-MSI (option C) platforms. For LA-ICP-MSI, the sample size is restricted by the inner diameter of the ablation chamber; this means, for example, that the HeLa cells should be cultivated on a slide <3 mm in diameter.

(A) **Combine the microlensed fiber device with the LDI-MSI platform**

● **TIMING 20 min**

▲ **CRITICAL** The TOF mass spectrometer used in this protocol is a home-built instrument, which is similar to most of the commercially available MALDI-TOF instruments. Note that the installation mode of the microlensed fiber device might differ slightly depending on the internal structure of the TOF mass analyzer.

(i) Mount the fiber pipe on a one-dimensional positioner, which is used to control the distance between the fiber tip and the sample surface (Fig. 2a). Start by placing the tip of the microlensed fiber on the sample surface. Then, pull the rear end of the fiber to the inner wall of the vacuum chamber.

(ii) Use a vacuum feedthrough to connect the fiber inside and outside of the vacuum chamber.

▲ **CRITICAL STEP** For this LDI-MSI platform, this step should be done before Step 10. That means it is necessary to connect the fiber inside and outside of the vacuum chamber before putting the back end of the fiber into the fiber clamp.

(iii) Mount the CCD camera with the microscope on the holder and then place it above the observing window. Adjust the position of the microscope so that the fiber and the sample are in the center of the field of view (Fig. 1j).

(iv) Turn on the laser. Check whether the laser successfully exits from the microlensed fiber with a CCD camera.

(B) **Combine the microlensed fiber device with the LA-ICP-MSI platform**

● **TIMING 20 min**

(i) Mount the fiber pipe on the 3D micropositioner, which is used to control the fiber-sample distance (through the $z$ axis) and the ablation area (through the $x$ and $y$ axes). Maintain an angle of 45° between the fiber and the sample surface.

(ii) Use the flexible silicone tube to connect the fiber pipe with the ablation chamber (Fig. 2b). Then, insert the microlensed fiber directly into the ablation chamber.

▲ **CRITICAL STEP** While inserting the microlensed fiber, the 3D micropositioner should be adjusted to make sure that the fiber does not contact the wall of the ablation chamber.

(iii) Put the sample on the sample stage and then put the stage into the ablation chamber from the lower branch of the chamber.
▲ **CRITICAL STEP** The sample size is restricted by the inner diameter of the ablation chamber.

(iv) Connect the ablation chamber to the ICP torch with a Teflon tube. The aerosol produced by the laser will be transmitted to the ICP-MS by the carrier gas.
▲ **CAUTION** The flame of the ICP source is very bright. Do not look directly at the flame without wearing protection glasses.

(v) Mount the CCD camera with the microscope and check the laser output from the fiber (follow Steps 13 and 14).

(C) **Combine the microlensed fiber device with the LA-ESI-MSI platform**
● **TIMING 20 min**

(i) Mount the fiber pipe on a one-dimensional positioner, which is used to control the distance between the fiber tip and the sample surface.

(ii) Use an ion transfer tube with a 50-mm extension. Heat the ion transfer tube with a cylinder-shaped ceramic heater (250 °C).
▲ **CAUTION** Keep your hands away from the ceramic heater when it is working.

(iii) Put the sample on a 3D positioner and set the distance between the sample surface and the ion transfer tube to 2 mm.

(iv) Set the distance between the nanoESI emitter and the ion transfer tube to 8 mm.
▲ **CRITICAL STEP** The nanoESI capillary used in this step is sharp. Any collision can cause the capillary tip to break.

(v) Mount the one-dimensional positioner (with the fiber pipe) above the sample stage. Set the distance between the microlensed fiber tip and the nanoESI emitter to 0.5 mm.

(vi) Mount the CCD camera with the microscope and check the laser output from the fiber (follow Steps 13 and 14).

### Measure the distance between the fiber tip and the sample surface

● **TIMING 10 min**

12. There are two possible ways to measure the distance:
    - Read the distance directly from the CCD monitor by comparing with the plotting scale and the diameter of the fiber (125 μm).
    - First, make the fiber tip just touch the sample surface by moving the micropositioner (the minimum step size of the positioner is 50 nm). Then, move the fiber away from the sample surface to a certain distance.

    ◆ **TROUBLESHOOTING**

### Sample preparation

● **TIMING Variable**

13. For full information about sample preparation, see the corresponding publications[22,24,26]. Some advice is included in Materials and Introduction. The most important consideration is that the samples be flat with a height variation of ≤2 μm.
    ◆ **TROUBLESHOOTING**

### MS imaging process

● **TIMING Variable**

14. Use a microscope to obtain the optical image of the region of interest of the sample surface.
    ▲ **CRITICAL STEP** It is important to obtain a clear image at this stage. After performing MSI experiments, the sample will be permanently damaged by the laser.
15. Put the sample onto the micropositioner. Restrict the region of interest of the sample surface and the microlensed fiber tip to the field of view of the CCD camera.
16. Check the distance between the fiber tip and the sample surface. Check the laser energy output from the microlensed fiber with the energy meter (Fig. 1e). This step determines the size of the sampling spot.
    ◆ **TROUBLESHOOTING**

17. Set the imaging area, the laser frequency and the moving speed of the sample on the micropositioner.
▲ **CRITICAL STEP** In this protocol, we use a self-written program to trigger the laser output and the moving of the sample. To avoid over-lapping sampling, we recommend controlling the laser frequency and the moving speed of the sample uniformly. For example, if the diameter of the sampling spot is 1 μm and the laser frequency is set to 10 Hz, then the moving speed of the sample should be set to 10 μm/s. That means the distance between each sampling spot is greater than or equal to the sampling spot size.
18. Acquire the imaging data. Normally, each data file includes the mass spectra and the total ion chromatogram of each row.
◆ **TROUBLESHOOTING**
19. During the imaging process, monitor the sample surface and the microlensed fiber tip through the CCD camera.
▲ **CRITICAL STEP** As mentioned above, the tolerance of the microlensed fiber to sample height fluctuations is ~2 microns. Excessive fluctuations can cause damage to the fiber. During the imaging process, it is necessary to monitor the position of the fiber.
◆ **TROUBLESHOOTING**
20. Compare the MS image with the optical image to get the precise location of the molecules or elements.

### Vent and pump for vacuum applications (required only for the LDI-MSI platform)

● **TIMING** Variable

21. Turn off all applied voltage to the mass spectrometer.
22. Turn off the turbo pump and the backing pump. Open the intake valve to reduce the vacuum of the TOF chamber.
23. Perform fiber cleaning, sample replacement and other operations.
24. Turn on the backing pump and the turbo pump for the next experiment.

### Clean the fiber

● **TIMING** 10 min

25. Remove the fiber pipe from the holder. Sink the fiber along with the pipe into ethanol and ultrasonically clean for 5 min. Then, re-install the fiber on the holder.

### Data analysis

● **TIMING** Variable

26. Acquire the full MS data of each sampling spot with an oscilloscope (for LDI-MSI), MassHunter software (Agilent Technologies) for LA-ICP-MSI and Xcalibur software (Thermo Fisher Scientific) for LA-ESI-MSI. The software will directly generate 2D data in which the *x*-coordinate is time and the *y*-coordinate is ion intensity.
27. Transform the data to an *xyz* format (the *x*-coordinate was the line number, the *y*-coordinate was the column number and the *z*-coordinate was ion intensity) according to the time required per line with a self-written program (LabVIEW 2018 and MATLAB 2022).
28. Produce the MS image by using a self-coded program (MATLAB 2022). In our work, all MS images are generated without the use of other image-processing steps, such as smoothing or interpolation.

## Troubleshooting

Troubleshooting advice can be found in Table 1. Although we have not yet seen an example of an unstable signal, we recognize that it might result from an unstable laser energy output or from fluctuations in the thickness of the sample.

**Table 1 | Troubleshooting table**

| Step | Problem | Possible reason | Solution |
|---|---|---|---|
| 9 | The flat end of the fiber is broken | The laser energy is too high | Reduce the laser energy and cut the fiber again to get a new flat end for laser coupling |
| 10 | The laser energy output from the fiber is much smaller than expected | The coupling efficiency is low; the fiber type is not suitable for the wavelength of the laser used | Precisely optimize the 3D positioner (micrometer precision adjustment); check the transmitting wavelength range of the fiber; check the material of the fiber |
| 12 | The view from the CCD camera is not clear | Reflective effect of the vacuum window | Optimize the angle of the light source of the microscope until you get a clear view |
| 13 | Too many cells on the plate; a single cell cannot be recognized | The concentration of cells produced during cell culture was too high | Use a dust-removing tool to carefully remove some of the cells from the plate |
| | | | Dilute the cells before applying a new sample |
| 16 | No laser output from the fiber | Fiber damage during the installation process | Check the connection of the fiber; check the laser coupling; change to another fiber |
| 18 | Collision between the fiber and the sample occurs during the MSI | The sample is not placed parallel to the sample stage; the height fluctuation of the sample surface is too large | Check the position of the sample. The sample should be placed parallel to the sample stage; prepare or choose a different sample that has less height fluctuation on the surface |
| 19 | A glisten effect occurs while observing with a CCD camera | Reflection effect of the ablation chamber | Optimize the angle of the light source |

## Timing

For the high-resolution imaging with a microlensed fiber, the time required is divided into eight parts: fabrication of the microlensed fiber (Steps 1–5), installation of the laser sampling device (Steps 6–10), combining the microlensed fiber with the MSI platform (Step 11A, B or C), measurement of the distance (Step 12), sample preparation (Step 13), MSI process (Steps 14–20), venting and pumping operation (Steps 21–24), fiber cleaning (Step 25) and data analysis (Steps 26–28).

Steps 1–5, fabrication of the microlensed fiber: 30 min. Multiple fibers can be fabricated with the grinding machine at the same time. The microlensed fiber can be maintained in the fiber box for further use. It is not necessary to repeat these steps before each MSI experiment.

Steps 6–10, installation of the microlensed fiber sampling device: 20 min

Step 11A, B or C, combining of the microlensed fiber sampling device with the MSI platform: 20 min

Step 12, measurement of the distance between the fiber tip and the sample surface: 10 min

Step 13, sample preparation

Cell culture: normally 24–36 h (the time spent depends on the time of drug incubation)

Mouse tissue section preparation: ~72 h (this step follows the normal paraffin section-preparing process)

Parsnip root section preparation: 10 min (fresh parsnip root from the market can be cut into the section without any treatment)

Standard copper grid sample preparation: 1 h

Steps 14–20, MSI process: variable, depending on the size of the imaging area (~1.5 h for the MSI result shown in Fig. 4b)

Steps 21–24, venting and pumping for vacuum applications: normally ~4 h but varies depending on the size of the vacuum chamber and the pumping speed of the turbo pump

Step 25, cleaning the fiber: 10 min

Steps 26–28, data analysis: variable

## Anticipated results

### Small-intestine imaging by using LA-ICP-MSI

For LA-ICP-MSI, we investigated the distributions of three photosensitive drugs (CuPc, ZnPc and CoTsPc) in the small intestine of mice (Fig. 4a–c). These drugs are commonly used in photodynamic therapy[55]. In photodynamic therapy, irradiation of tumor sites with light of specific wavelength can activate photosensitive drugs that selectively concentrate in tumor tissues and trigger photochemical reactions to destroy the tumor. In this experiment, the drugs were administered by gavage, and the samples were fixed, embedded and sliced as described in Materials (see also Fig. 4a), while the detailed steps for MS imaging are described in the Procedure. Figure 4b shows the optical image of the small-intestine section. By changing the applied laser energy and the distance between the fiber tip and the sample surface, MSI was carried out at two spatial resolutions: 0.5 and 5 µm (Fig. 4c). The figure shows that the MSI results are clearer and more accurate at the higher spatial resolution. Figure 4d shows MS images corresponding to each of the three drugs analyzed in the yellow outlined region of Fig. 4c. Of the three photosensitive drugs, CoTsPc has the widest distribution, which represents the maximum drug absorption. Its efficient intestinal absorption could be ascribed to the high water solubility of the drug. All three drugs have their highest concentration in the intestinal villi tissues, which confirms that the large surface area of the villi is the key to small intestinal absorption. Despite the differences in the concentration distribution, all three drugs show their highest concentrations in the epithelia and blood capillaries of the intestine, confirming absorption via epithelia and transportion to other parts of the body by the blood capillaries. Goblet cells are clearly visible in the MS image with the spatial resolution of 0.5 µm.

### Parsnip root imaging by using LA-ESI-MSI

For LA-ESI-MSI, a parsnip root slice was studied. Figure 4e shows the optical image of the imaging area. We performed the high-resolution MSI with the microlensed fiber in the area inside the dotted line (2 mm × 2 mm) and compared the results of experiments performed at two different spatial resolutions (Fig. 4f–j shows images obtained by collecting data for different metabolites; each metabolite was analyzed at two different resolutions). Each pixel represents the MS signal of a microlensed fiber sampling crater with a diameter of ~5 µm, whereas the pixel representing the MS signal achieved with traditional LA-ESI-MSI has a diameter of ~100 µm. From the high-resolution MS image, the precise location of different molecules can be obtained. For example, because of the fuzzy boundary in the low-resolution MS image, it is difficult to recognize whether the metabolite with $m/z$ = 365.1024 is distributed only in the phloem or both the phloem and cortex. By comparing the high-resolution MS image with the optical image, we can clearly see that it is only distributed in the phloem. Because of the high-throughput advantage of MSI, all metabolites can be analyzed simultaneously. After the imaging process, the MS image of a specific metabolite can be obtained by data processing of the corresponding $m/z$ value.

### Single-cell imaging

Traditional single-cell MS analysis refers to stochastic average values masked by bulk measurements, resulting in the loss of information related to intercellular chemical heterogeneities in large cell populations[56–62]. However, the development of single-cell imaging makes it possible to understand differences in chemical composition between different organelles. With plenty of advantages such as direct solid analysis, little or no sample-preparation procedures, reduced risk of contamination, low sample consumption, rapid analysis and sampling in microzones, laser-based sampling is regarded as one of the most versatile sampling techniques for single-cell MSI. The biggest challenge of single-cell imaging for laser-based MSI is the spatial resolution, which can be solved by using a microlensed fiber. In this protocol, we develop the strategies for the MSI of single adherent cells growing on quartz wafers with the LDI-MSI platform and LA-ICP-MSI platform that have been introduced above.

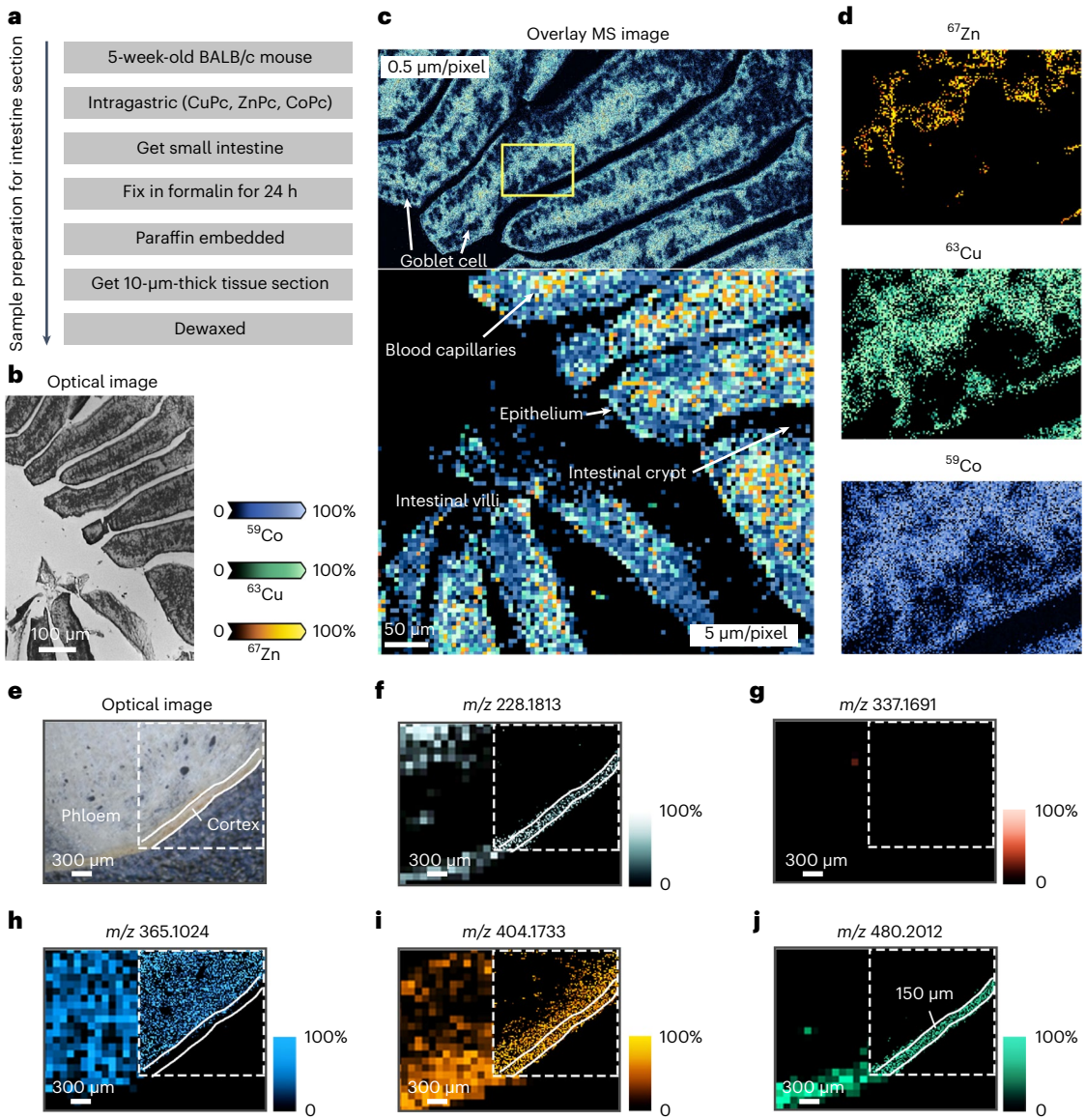


**Fig. 4 | Tissue imaging achieved by laser-based MSI with a microlensed fiber.** **a**, Small-intestine tissue section preparation. **b**, Optical image of the imaging area. **c**, LA-ICP-MSI result of three photosensitive drugs of different spatial resolution with a microlensed fiber. Upper: 0.5 μm/pixel; lower: 5 μm/pixel. **d**, Separate MS images of zinc, copper and cobalt of the outlined region in yellow in **c**. **e**, Optical image of a parsnip root section sample. **f**–**j**, Different metabolite imaging results with the LA-ESI-MSI platform. The outer area is achieved with a traditional laser-focusing method, whereas the inner area within the dotted line is achieved with the microlensed fiber. Images in **b**–**d** adapted with permission from ref. 26, American Chemical Society.

### LDI-MSI of acriflavine in a HeLa cell

Figure 5a shows the optical and atomic force microscope (AFM) image of a HeLa cell after laser scanning with a microlensed fiber. Sampling craters on the cell can be observed clearly. From the AFM image, the diameter of the ablated spots can be defined as ~350 nm. Figure 5b shows the results obtained after single-cell LDI-MSI of HeLa cells cultured with acriflavine[63]. Treatment with acriflavine was chosen because it is a cancer drug that has known biological activity and a known photoionization mechanism. The anticipated ion peak of $[M\text{-}Cl]^+$ was detected at $m/z = 224$. The MS images of the drug distribution match well with the optical image of the cell, showing that most of the drug is concentrated in the cytoplasm. Furthermore, traces of drugs are also detected in the nucleolus within the nucleus.

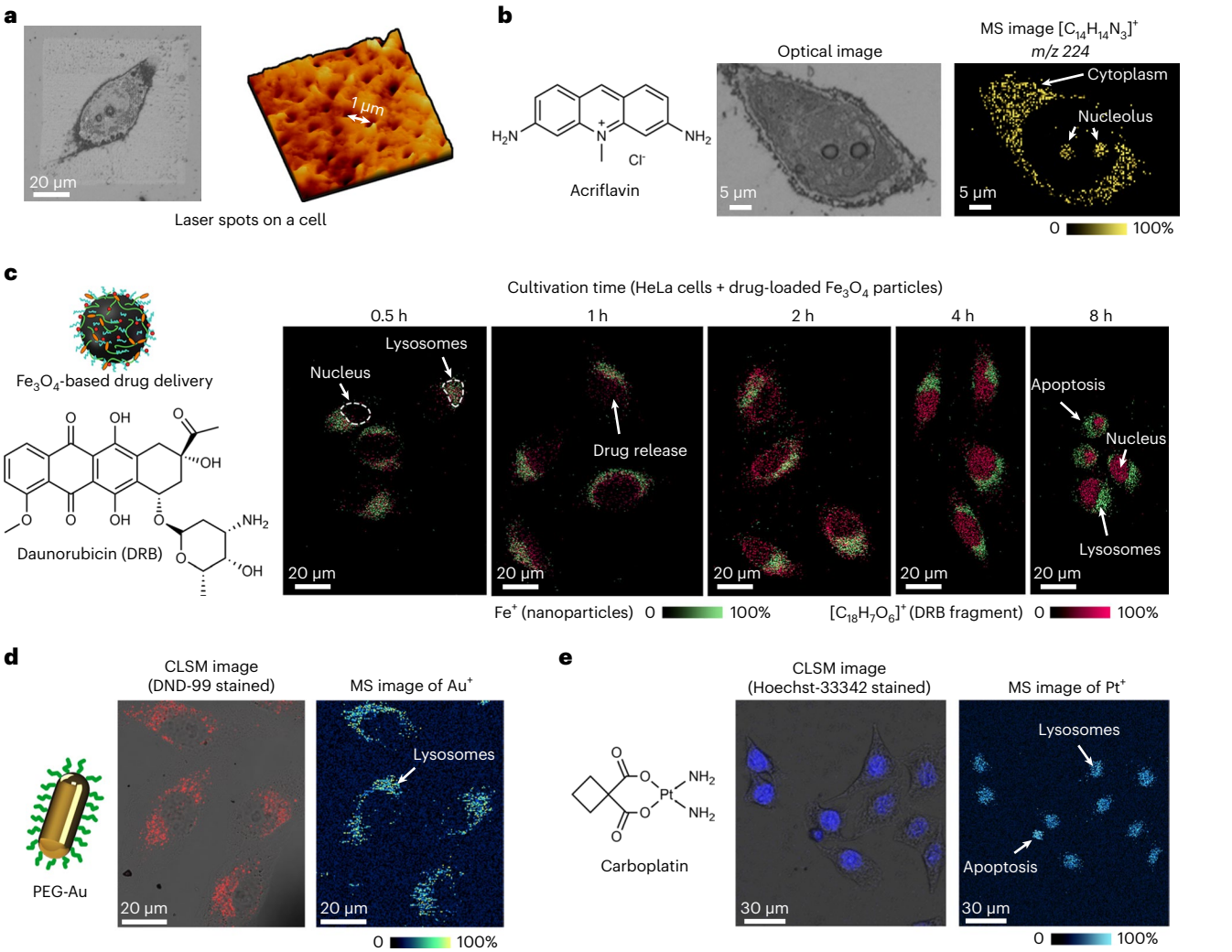


**Fig. 5 | Single-cell imaging achieved by laser-based MSI with the microlensed fiber. a**, Sampling craters on a single HeLa cell. The atomic force microscopy image indicates that the diameter of the ablated craters is ~350 nm. **b**, MSI of acriflavine in a HeLa cell with the LDI-MSI platform. **c**, MSI of the anticancer drug-loaded nanoparticles in HeLa cells with different culture time. **d**, MSI of gold nanorods in HeLa cells with the LA-ICP-MSI platform. **e**, MSI of carboplatin drugs in HeLa cells with the LA-ICP-MSI platform. CLSM, confocal laser scanning microscopy. Images in **a**–**c** adapted with permission from ref. 24, Wiley. Images in **d** and **e** adapted with permission from ref. 26, American Chemical Society.

### Imaging in situ release of daunorubicin

In Fig. 5c, we show imaging results relating to a targeted drug delivery system based on nanoparticles ($Fe_3O_4$) designed for in situ release of drug (daunorubicin, DRB) in cells. To decipher the interactions between anticancer drugs and cancer cells, MSI was performed on HeLa cells with drug-loaded nanoparticles at different culture times from 0.5 to 8 h. In the MSI results, the green pixels represent the distribution of $Fe^+$ (nanoparticles), while the red pixels represent the location of DRB. This was possible because we analyzed for $m/z = 56$ ($Fe^+$) and 321 (DRB fragment). By comparing with the fluorescence image of the lysosome and nucleus dye (DND-99 and Hoechst-33342), the subcellular distribution of drugs and nanocarriers can be determined (Supplementary Fig. 12). After cultivation for 0.5 h, both the anticancer drugs and the carriers have the same distribution: they are found only in the lysosomes. However, after 2 h, a small trace of DRB can be found in the nucleus, which indicates the start of drug release. As the cultivation time increases to 4 h, drugs gradually escape the nanoparticles in lysosomes and enter the cytoplasm, where they eventually accumulate in the nucleus. The gradual

transfer of the anticancer drug from lysosomes to nuclei is clearly visible from the MSI results. Simultaneous monitoring of the cell morphology showed substantial cell shrinkage and apoptosis after 8 h. This suggests that DRB acts in the nucleus and that the outcome is apoptosis of cancer cells.

### Gold nanorods and carboplatin drugs by LA-ICP-MSI

The LA-ICP-MSI platform equipped with the microlensed fiber can also be used for single-cell imaging. By comparing confocal laser scanning microscopy images in which the cells were stained with lysosome tracker DND-99 and nucleus dye Hoechst-33342, the gold nanorods and carboplatin drugs were found in lysosomes and the nucleus, respectively, of the HeLa cells (Fig. 5d,e).

In summary, we introduce an economic and universal technique for subcellular laser-based MSI by using a microlensed fiber. It is suggested that existing laser-based MSI platforms can achieve much higher spatial resolution by introducing the microlensed fiber module with simple modifications. This approach has the potential to improve the resolution of MS imaging in drug discovery, clinical research, biochemistry and molecular biology.

## Reporting summary

Further information on research design is available in the Nature Portfolio Reporting Summary linked to this article.

## Data availability

The data presented in Anticipated results are from previous publications[22,24,26] and are available from the corresponding authors. The figures have been rearranged and embedded.

## Code availability

The LabVIEW and MATLAB programs are available from https://github.com/yfmeng1121/SmarAct-micropositioner-control.

Received: 20 October 2022; Accepted: 2 May 2023;
Published online: 21 July 2023

## References

1. McDonnell, L. A. & Heeren, R. M. A. Imaging mass spectrometry. *Mass Spectrom. Rev.* **26**, 606–643 (2007).
2. Seeley, E. H. & Caprioli, R. M. MALDI imaging mass spectrometry of human tissue: method challenges and clinical perspectives. *Trends Biotechnol.* **29**, 136–143 (2011).
3. Buchberger, A. R., DeLaney, K., Johnson, J. & Li, L. Mass spectrometry imaging: a review of emerging advancements and future insights. *Anal. Chem.* **90**, 240–265 (2018).
4. Wu, C., Dill, A. L., Eberlin, L. S., Cooks, R. G. & Ifa, D. R. Mass spectrometry imaging under ambient conditions. *Mass Spectrom. Rev.* **32**, 218–243 (2013).
5. Lanni, E. J., Rubakhin, S. S. & Sweedler, J. V. Mass spectrometry imaging and profiling of single cells. *J. Proteom.* **75**, 5036–5051 (2012).
6. Unsihuay, D., Sanchez, D. M. & Laskin, J. Quantitative mass spectrometry imaging of biological systems. *Annu. Rev. Phys. Chem.* **72**, 307–329 (2021).
7. Doble, P. A., de Vega, R. G., Bishop, D. P., Hare, D. J. & Clases, D. Laser ablation–inductively coupled plasma–mass spectrometry imaging in biology. *Chem. Rev.* **121**, 11769–11822 (2021).
8. Chen, Y., Xie, Y., Li, L., Wang, Z. & Yang, L. Advances in mass spectrometry imaging for toxicological analysis and safety evaluation of pharmaceuticals. *Mass Spectrom. Rev.* **22**, e21807 (2022).
9. Granborg, J. R., Handler, A. M. & Janfelt, C. Mass spectrometry imaging in drug distribution and drug metabolism studies—principles, applications and perspectives. *Trends Anal. Chem.* **146**, 116482 (2022).
10. Ma, X. & Fernández, F. M. Advances in mass spectrometry imaging for spatial cancer metabolomics. *Mass Spectrom. Rev.* **6**, e21804 (2022).
11. Chen, S. et al. Mass spectrometry imaging reveals the sub-organ distribution of carbon nanomaterials. *Nat. Nanotechnol.* **10**, 176–182 (2015).
12. Xue, J. et al. Mass spectrometry imaging of the in situ drug release from nanocarriers. *Sci. Adv.* **4**, eaat9039 (2018).
13. Yang, J. et al. Polydopamine-modified substrates for high-sensitivity laser desorption ionization mass spectrometry imaging. *ACS Appl. Mater. Interfaces* **11**, 46140–46148 (2019).
14. Neumann, E. K., Comi, T. J., Rubakhin, S. S. & Sweedler, J. V. Lipid heterogeneity between astrocytes and neurons revealed by single-cell MALDI-MS combined with immunocytochemical classification. *Angew. Chem. Int. Ed. Engl.* **58**, 5910–5914 (2019).
15. Caprioli, R. M., Farmer, T. B. & Gile, J. Molecular imaging of biological samples: localization of peptides and proteins using MALDI-TOF MS. *Anal. Chem.* **69**, 4751–4760 (1997).
16. Cornett, D. S., Reyzer, M. L., Chaurand, P. & Caprioli, R. M. MALDI imaging mass spectrometry: molecular snapshots of biochemical systems. *Nat. Methods* **4**, 828–833 (2007).
17. Liu, R. et al. Metal stable isotope tagging: renaissance of radioimmunoassay for multiplex and absolute quantification of biomolecules. *Acc. Chem. Res.* **49**, 775–783 (2016).
18. Drescher, D. et al. Quantitative imaging of gold and silver nanoparticles in single eukaryotic cells by laser ablation ICP-MS. *Anal. Chem.* **84**, 9684–9688 (2012).
19. Wang, H. A. O. et al. Fast chemical imaging at high spatial resolution by laser ablation inductively coupled plasma mass spectrometry. *Anal. Chem.* **85**, 10107–10116 (2013).
20. Stolee, J. A., Shrestha, B., Mengistu, G. & Vertes, A. Observation of subcellular metabolite gradients in single cells by laser ablation electrospray ionization mass spectrometry. *Angew. Chem. Int. Ed. Engl.* **51**, 10386–10389 (2012).
21. Nemes, P. & Vertes, A. Laser ablation electrospray ionization for atmospheric pressure, in vivo, and imaging mass spectrometry. *Anal. Chem.* **79**, 8098–8106 (2007).
22. Meng, Y., Song, X. & Zare, R. N. Laser ablation electrospray ionization achieves 5 μm resolution using a microlensed fiber. *Anal. Chem.* **94**, 10278–10282 (2022).
23. Wang, T. et al. Perspective on advances in laser-based high-resolution mass spectrometry imaging. *Anal. Chem.* **92**, 543–553 (2020).

24. Meng, Y. et al. Micro-lensed fiber laser desorption mass spectrometry imaging reveals subcellular distribution of drugs within single cells. *Angew. Chem. Int. Ed. Engl.* **59**, 17864–17871 (2020).
25. Meng, Y., Ma, S., Zhang, Z. & Hang, W. 3D nanoscale chemical imaging of core–shell microspheres via microlensed fiber laser desorption postionization mass spectrometry. *Anal. Chem.* **92**, 9916–9921 (2020).
26. Meng, Y., Gao, C., Lu, Q., Ma, S. & Hang, W. Single-cell mass spectrometry imaging of multiple drugs and nanomaterials at organelle level. *ACS Nano* **15**, 13220–13229 (2021).
27. Li, X. et al. Nanoscale three-dimensional imaging of drug distributions in single cells via laser desorption post-ionization mass spectrometry. *J. Am. Chem. Soc.* **143**, 21648–21656 (2021).
28. Hanley, L. & Zimmermann, R. Light and molecular ions: the emergence of vacuum UV single-photon ionization in MS. *Anal. Chem.* **81**, 4174–4182 (2009).
29. Zenobi, R. & Knochenmuss, R. Ion formation in MALDI mass spectrometry. *Mass Spectrom. Rev.* **17**, 337–366 (1998).
30. Sylvester, P. (ed.) in *Laser Ablation ICP-MS in the Earth Sciences: Current Practices and Outstanding Issues* Vol. 40, Ch. 5, 67–78 (Mineralogical Association of Canada, 2008).
31. Motelica-Heino, M., Le Coustumer, P. & Donard, O. F. X. Micro- and macro-scale investigation of fractionation and matrix effects in LA-ICP-MS at 1064 nm and 266 nm on glassy materials. *J. Anal. Spectrom.* **16**, 542–550 (2001).
32. Shrestha, B. & Vertes, A. In situ metabolic profiling of single cells by laser ablation electrospray ionization mass spectrometry. *Anal. Chem.* **81**, 8265–8271 (2009).
33. Stolee, J. A. & Vertes, A. Toward single-cell analysis by plume collimation in laser ablation electrospray ionization mass spectrometry. *Anal. Chem.* **85**, 3592–3598 (2013).
34. Passarelli, M. K. et al. The 3D OrbiSIMS—label-free metabolic imaging with subcellular lateral resolution and high mass-resolving power. *Nat. Methods* **14**, 1175–1183 (2017).
35. Takáts, Z., Wiseman, J. M., Gologan, B. & Cooks, R. G. Mass spectrometry sampling under ambient conditions with desorption electrospray ionization. *Science* **306**, 471–473 (2004).
36. Eberlin, L. S. et al. Molecular assessment of surgical-resection margins of gastric cancer by mass-spectrometric imaging. *Proc. Natl Acad. Sci. USA* **111**, 2436–2441 (2014).
37. Eberlin, L. S. et al. Ambient mass spectrometry for the intraoperative molecular diagnosis of human brain tumors. *Proc. Natl Acad. Sci. USA* **110**, 1611–1616 (2013).
38. Wedlock, L. E. et al. NanoSIMS multi-element imaging reveals internalisation and nucleolar targeting for a highly-charged polynuclear platinum compound. *Chem. Commun.* **49**, 6944–6946 (2013).
39. Senyo, S. E. et al. Mammalian heart renewal by pre-existing cardiomyocytes. *Nature* **493**, 433–436 (2012).
40. Yuan, Z. et al. SEAM is a spatial single nuclear metabolomics method for dissecting tissue microenvironment. *Nat. Methods* **18**, 1223–1232 (2021).
41. Wiseman, J. M. et al. Desorption electrospray ionization mass spectrometry: imaging drugs and metabolites in tissues. *Proc. Natl Acad. Sci. USA* **105**, 18120–18125 (2008).
42. Yin, R., Burnum-Johnson, K. E., Sun, X., Dey, S. K. & Laskin, J. High spatial resolution imaging of biological tissues using nanospray desorption electrospray ionization mass spectrometry. *Nat. Protoc.* **14**, 3445–3470 (2019).
43. Kompauer, M., Heiles, S. & Spengler, B. Atmospheric pressure MALDI mass spectrometry imaging of tissues and cells at 1.4-μm lateral resolution. *Nat. Methods* **14**, 90–96 (2016).
44. Zavalin, A. et al. Direct imaging of single cells and tissue at sub-cellular spatial resolution using transmission geometry MALDI MS. *J. Mass Spectrom.* **47**, 1473–1481 (2012).
45. Spivey, E. C., McMillen, J. C., Ryan, D. J., Spraggins, J. M. & Caprioli, R. M. Combining MALDI-2 and transmission geometry laser optics to achieve high sensitivity for ultra-high spatial resolution surface analysis. *J. Mass Spectrom.* **54**, 366–370 (2019).
46. Niehaus, M., Soltwisch, J., Belov, M. E. & Dreisewerd, K. Transmission-mode MALDI-2 mass spectrometry imaging of cells and tissues at subcellular resolution. *Nat. Methods* **16**, 925–931 (2019).
47. Yin, Z. et al. Chemical and topographical single-cell imaging by near-field desorption mass spectrometry. *Angew. Chem. Int. Ed. Engl.* **58**, 4541–4546 (2019).
48. Liang, Z. et al. Tip-enhanced ablation and ionization mass spectrometry for nanoscale chemical analysis. *Sci. Adv.* **3**, eaaq1059 (2017).
49. Schmitz, T. A., Gamez, G., Setz, P. D., Zhu, L. & Zenobi, R. Towards nanoscale molecular analysis at atmospheric pressure by a near-field laser ablation ion trap/time-of-flight mass spectrometer. *Anal. Chem.* **80**, 6537–6544 (2008).
50. Wang, J. et al. Vacuum ultraviolet laser desorption/ionization mass spectrometry imaging of single cells with submicron craters. *Anal. Chem.* **90**, 10009–10015 (2018).
51. Kuznetsov, I. et al. Three-dimensional nanoscale molecular imaging by extreme ultraviolet laser ablation mass spectrometry. *Nat. Commun.* **6**, 6944 (2015).
52. Giesen, C. et al. Highly multiplexed imaging of tumor tissues with subcellular resolution by mass cytometry. *Nat. Methods* **11**, 417–422 (2014).
53. Lu, Q., Xu, Z., You, X., Ma, S. & Zenobi, R. Atmospheric pressure mass spectrometry imaging using laser ablation, followed by dielectric barrier discharge ionization. *Anal. Chem.* **93**, 6232–6238 (2021).
54. Lu, Q., Guan, X., You, X., Xu, Z. & Zenobi, R. High-spatial resolution atmospheric pressure mass spectrometry imaging using fiber probe laser ablation-dielectric barrier discharge ionization. *Anal. Chem.* **93**, 14694–14700 (2021).
55. Dolmans, D. E. J. G. J., Fukumura, D. & Jain, R. K. Photodynamic therapy for cancer. *Nat. Rev. Cancer* **3**, 380–387 (2003).
56. Gong, X. et al. Single cell analysis with probe ESI-mass spectrometry: detection of metabolites at cellular and subcellular levels. *Anal. Chem.* **86**, 3809–3816 (2014).
57. Fujii, T. et al. Direct metabolomics for plant cells by live single-cell mass spectrometry. *Nat. Protoc.* **10**, 1445–1456 (2015).
58. Zhu, H. et al. Single-neuron identification of chemical constituents, physiological changes, and metabolism using mass spectrometry. *Proc. Natl Acad. Sci. USA* **114**, 2586–2591 (2017).
59. Hu, K., Nguyen, T. D. K., Rabasco, S., Oomen, P. E. & Ewing, A. G. Chemical analysis of single cells and organelles. *Anal. Chem.* **93**, 41–71 (2021).
60. Xu, S., Liu, M., Bai, Y. & Liu, H. Multi-dimensional organic mass cytometry: simultaneous analysis of proteins and metabolites on single cells. *Angew. Chem. Int. Ed. Engl.* **60**, 1806–1812 (2021).
61. Zenobi, R. Single-cell metabolomics: analytical and biological perspectives. *Science* **342**, 1243259 (2013).
62. Comi, T. J., Do, T. D., Rubakhin, S. S. & Sweedler, J. V. Categorizing cells on the basis of their chemical profiles: progress in single-cell mass spectrometry. *J. Am. Chem. Soc.* **139**, 3920–3929 (2017).
63. Kim, S. G. et al. Enhanced anti-tumour effects of acriflavine in combination with guanosine in mice. *J. Pharm. Pharmacol.* **49**, 216–222 (1997).


## Acknowledgements

This work is supported by the Natural Science Foundation of China (21974116 and 22027808) and the Air Force Office of Scientific Research through the Multidisciplinary University Research Initiative (MURI) program (AFOSR FA9550-21-1-0170).

## Author contributions

W.H., R.N.Z. and Y.M. developed the procedure. Y.M. performed the imaging experiments and processed the data. The manuscript was written by all authors.

## Competing interests

The authors declare no competing interests.

## Additional information

**Supplementary information** The online version contains supplementary material available at https://doi.org/10.1038/s41596-023-00848-1.

**Correspondence and requests for materials** should be addressed to Wei Hang or Richard N. Zare.

**Peer review information** *Nature Protocols* thanks Li Yang and the other, anonymous, reviewer(s) for their contribution to the peer review of this work.



## Related links

**Key references using this protocol**

Meng, Y. et al. *Angew. Chem. Int. Ed. Engl.* **59**, 17864–17871 (2020): https://doi.org/10.1002/anie.202002151

Meng, Y. et al. *ACS Nano* **15**, 13220–13229 (2021): https://doi.org/10.1021/acsnano.1c02922

Meng, Y. et al. *Anal. Chem.* **94**, 10278–10282 (2022): https://doi.org/10.1021/acs.analchem.2c01942

nature portfolio

Corresponding author(s): Richard N. Zare, Wei Hang

Last updated by author(s): 2023-04-17

# Reporting Summary

Nature Portfolio wishes to improve the reproducibility of the work that we publish. This form provides structure for consistency and transparency in reporting. For further information on Nature Portfolio policies, see our Editorial Policies and the Editorial Policy Checklist.

Please do not complete any field with "not applicable" or n/a. Refer to the help text for what text to use if an item is not relevant to your study.
For final submission: please carefully check your responses for accuracy; you will not be able to make changes later.

## Statistics

For all statistical analyses, confirm that the following items are present in the figure legend, table legend, main text, or Methods section.

n/a Confirmed

- [x] The exact sample size (*n*) for each experimental group/condition, given as a discrete number and unit of measurement
- [x] A statement on whether measurements were taken from distinct samples or whether the same sample was measured repeatedly
- [x] The statistical test(s) used AND whether they are one- or two-sided
  *Only common tests should be described solely by name; describe more complex techniques in the Methods section.*
- [x] A description of all covariates tested
- [x] A description of any assumptions or corrections, such as tests of normality and adjustment for multiple comparisons
- [x]
- [ ] A full description of the statistical parameters including central tendency (e.g. means) or other basic estimates (e.g. regression coefficient) AND variation (e.g. standard deviation) or associated estimates of uncertainty (e.g. confidence intervals)
- [x] For null hypothesis testing, the test statistic (e.g. *F*, *t*, *r*) with confidence intervals, effect sizes, degrees of freedom and *P* value noted
  *Give P values as exact values whenever suitable.*
- [x] For Bayesian analysis, information on the choice of priors and Markov chain Monte Carlo settings
- [x] For hierarchical and complex designs, identification of the appropriate level for tests and full reporting of outcomes
- [x] Estimates of effect sizes (e.g. Cohen's *d*, Pearson's *r*), indicating how they were calculated

*Our web collection on statistics for biologists contains articles on many of the points above.*

## Software and code

Policy information about availability of computer code

| | |
|---|---|
| Data collection | MassHunter software (Agilent Technologies, CA, US) , Xcalibur software (Thermo Fishier Scientific, MA, US) |
| Data analysis | MATLAB 2022 |

For manuscripts utilizing custom algorithms or software that are central to the research but not yet described in published literature, software must be made available to editors and reviewers. We strongly encourage code deposition in a community repository (e.g. GitHub). See the Nature Portfolio guidelines for submitting code & software for further information.

## Data

Policy information about availability of data

All manuscripts must include a data availability statement. This statement should provide the following information, where applicable:

- Accession codes, unique identifiers, or web links for publicly available datasets
- A description of any restrictions on data availability
- For clinical datasets or third party data, please ensure that the statement adheres to our policy

The data presented in 'Anticipated results' were from the previously published researches in references 22, 24, and 26; Data are available from the corresponding authors. The figures have been rearranged and embedded.

## Human research participants

Policy information about studies involving human research participants and Sex and Gender in Research.

| | |
|---|---|
| Reporting on sex and gender | NA |
| Population characteristics | NA |
| Recruitment | NA |
| Ethics oversight | NA |

Note that full information on the approval of the study protocol must also be provided in the manuscript.

# Field-specific reporting

Please select the one below that is the best fit for your research. If you are not sure, read the appropriate sections before making your selection.

◉ Life sciences ○ Behavioural & social sciences ○ Ecological, evolutionary & environmental sciences

# Life sciences study design

All studies must disclose on these points even when the disclosure is negative.

| | |
|---|---|
| Sample size | This is a method development project. The focus of this study was not on sample size. |
| Data exclusions | No data were excluded. |
| Replication | Every sample is unique so there is no replication. |
| Randomization | Randomization was not relevant. |
| Blinding | Blinding was not relevant. |

# Behavioural & social sciences study design

All studies must disclose on these points even when the disclosure is negative.

| | |
|---|---|
| Study description | |
| Research sample | |
| Sampling strategy | |
| Data collection | |
| Timing | |
| Data exclusions | |
| Non-participation | |
| Randomization | |

# Ecological, evolutionary & environmental sciences study design

All studies must disclose on these points even when the disclosure is negative.

| | |
|---|---|
| Study description | |
| Research sample | |
| Sampling strategy | |
| Data collection | |
| Timing and spatial scale | |
| Data exclusions | |
| Reproducibility | |
| Randomization | |

Blinding

Did the study involve field work? ○ Yes ○ No

## Field work, collection and transport

Field conditions

Location

Access & import/export

Disturbance

# Reporting for specific materials, systems and methods

We require information from authors about some types of materials, experimental systems and methods used in many studies. Here, indicate whether each material, system or method listed is relevant to your study. If you are not sure if a list item applies to your research, read the appropriate section before selecting a response.

### Materials & experimental systems

| n/a | Involved in the study |
|---|---|
| ○ | ○ Antibodies |
| ○ | ● Eukaryotic cell lines |
| ○ | ○ Palaeontology and archaeology |
| ○ | ● Animals and other organisms |
| ○ | ○ Clinical data |
| ○ | ○ Dual use research of concern |

### Methods

| n/a | Involved in the study |
|---|---|
| ○ | ○ ChIP-seq |
| ○ | ○ Flow cytometry |
| ○ | ○ MRI-based neuroimaging |

## Antibodies

Antibodies used

Validation

## Eukaryotic cell lines

Policy information about cell lines and Sex and Gender in Research

Cell line source(s): HeLa cells (human cervical cancer cells) were obtained from Cell bank, Shanghai institute of life sciences, Chinese Academy of

Authentication

Mycoplasma contamination

Commonly misidentified lines (See ICLAC register)

## Palaeontology and Archaeology

Specimen provenance

Specimen deposition

Dating methods

☐ Tick this box to confirm that the raw and calibrated dates are available in the paper or in Supplementary Information.

Ethics oversight

Note that full information on the approval of the study protocol must also be provided in the manuscript.

## Animals and other research organisms

Policy information about studies involving animals; ARRIVE guidelines recommended for reporting animal research, and Sex and Gender in Research

| | |
|---|---|
| Laboratory animals | BALB/c mice (female) of 5-week-old used in this experiment were provide by Xiamen University Laboratory Animal Center. All animal |
| Wild animals | No wild animals were used. |
| Reporting on sex | Sex does not affect to the results. |
| Field-collected samples | |
| Ethics oversight | |

Note that full information on the approval of the study protocol must also be provided in the manuscript.

## Clinical data

Policy information about clinical studies

All manuscripts should comply with the ICMJE guidelines for publication of clinical research and a completed CONSORT checklist must be included with all submissions.

| | |
|---|---|
| Clinical trial registration | |
| Study protocol | |
| Data collection | |
| Outcomes | |

## Dual use research of concern

Policy information about dual use research of concern

### Hazards

Could the accidental, deliberate or reckless misuse of agents or technologies generated in the work, or the application of information presented in the manuscript, pose a threat to:

| No | Yes | |
|---|---|---|
| ○ | ○ | Public health |
| ○ | ○ | National security |
| ○ | ○ | Crops and/or livestock |
| ○ | ○ | Ecosystems |
| ○ | ○ | Any other significant area |

### Experiments of concern

Does the work involve any of these experiments of concern:

| No | Yes | |
|---|---|---|
| ○ | ○ | Demonstrate how to render a vaccine ineffective |
| ○ | ○ | Confer resistance to therapeutically useful antibiotics or antiviral agents |
| ○ | ○ | Enhance the virulence of a pathogen or render a nonpathogen virulent |
| ○ | ○ | Increase transmissibility of a pathogen |
| ○ | ○ | Alter the host range of a pathogen |
| ○ | ○ | Enable evasion of diagnostic/detection modalities |
| ○ | ○ | Enable the weaponization of a biological agent or toxin |
| ○ | ○ | Any other potentially harmful combination of experiments and agents |

## ChIP-seq

### Data deposition

☐ Confirm that both raw and final processed data have been deposited in a public database such as GEO.

☐ Confirm that you have deposited or provided access to graph files (e.g. BED files) for the called peaks.

| | |
|---|---|
| Data access links<br>*May remain private before publication.* | |
| Files in database submission | |
| Genome browser session<br>(e.g. UCSC ) | |

### Methodology

Replicates

Sequencing depth

Antibodies

Peak calling parameters

Data quality

Software

## Flow Cytometry

### Plots

Confirm that:

☐ The axis labels state the marker and fluorochrome used (e.g. CD4-FITC).

☐ The axis scales are clearly visible. Include numbers along axes only for bottom left plot of group (a 'group' is an analysis of identical markers).

☐ All plots are contour plots with outliers or pseudocolor plots.

☐ A numerical value for number of cells or percentage (with statistics) is provided.

### Methodology

Sample preparation

Instrument

Software

Cell population abundance

Gating strategy

☐ Tick this box to confirm that a figure exemplifying the gating strategy is provided in the Supplementary Information.

## Magnetic resonance imaging

### Experimental design

Design type

Design specifications

Behavioral performance measures

### Acquisition

Imaging type(s)

Field strength

Sequence & imaging parameters

Area of acquisition

Diffusion MRI ○ Used ○ Not used

### Preprocessing

Preprocessing software

Normalization

Normalization template

Noise and artifact removal

Volume censoring

### Statistical modeling & inference

Model type and settings

Effect(s) tested

Specify type of analysis: ○ Whole brain ○ ROI-based ○ Both

Statistic type for inference (See Eklund et al. 2016 )

Correction

## Models & analysis

n/a | Involved in the study

- Functional and/or effective connectivity
- Graph analysis
- Multivariate modeling or predictive analysis

Functional and/or effective connectivity

Graph analysis

Multivariate modeling and predictive analysis